$K\alpha$ x-ray satellite lines of Si induced in collisions with 1–3-MeV protons

Matjaž Kavčič
J. Stefan Institute, P.O. Box 3000, SI-1001 Ljubljana, Slovenia
(Received 23 May 2003; published 28 August 2003)

The $K\alpha$ x-ray emission spectra of Si bombarded by 1–3-MeV protons were measured with a crystal spectrometer in Johansson geometry, enabling energy resolution below the natural linewidth of the measured $K\alpha$ line. The $K\alpha L^1$ and $K\alpha L^2$ ($K\alpha L^{1,2}$) x-ray satellite lines appearing in these spectra as a result of the radiative decay of atomic states with one hole in the K shell and one or two in the L subshells were precisely measured. The energies and intensities of the main components that could be resolved within the satellite lines are given. It has been demonstrated that the latter do not depend on proton energy and are essentially the same as in photon-induced spectra. The overall $K\alpha L^1$ satellite intensity relative to the $K\alpha$ diagram line has been used to deduce the L-shell ionization probabilities induced in near-central proton collisions. The experimental values were compared to the theoretical values calculated with the semiclassical approximation, with the three-body classical trajectory Monte Carlo model, and the classical binary-encounter-based geometrical model.

DOI: 10.1103/PhysRevA.68.022713 PACS number(s): 32.80.Hd, 32.30.Rj, 32.70.−n

I. INTRODUCTION

An excited atom with a single $1s$ shell vacancy emits an Auger electron or a photon during the deexcitation process. The photons emitted in these radiative transitions correspond to characteristic diagram lines in the K x-ray spectra of the particular element. When the $1s$ vacancy is accompanied by an additional vacancy in one of the higher atomic shells, these photons are slightly shifted to higher energies and correspond to the so-called satellite lines in the K x-ray spectrum. When the $1s$ vacancy is accompanied by one or more L-shell vacancies, the satellite lines are denoted as KL^N, where N is the number of L-shell vacancies. For low-Z elements, the energy shift of the $K\alpha L^1$ satellite relative to the parent $K\alpha$ diagram line is 10–20 eV. Therefore, in order to be able to resolve the satellite lines, high-resolution x-ray spectroscopy employing crystal spectrometers is required.

The creation of multiple inner-shell vacancies in an atom is actually the dominant feature in the collisions of heavy ions with low-Z atoms. Due to very strong Coulomb interaction between the projectile and the target electrons, the ion-induced x-ray spectra exhibit rich satellite structure with very intense high-order satellites. Satellite lines can be observed also in collisions with protons or electrons but the satellite intensities are much weaker and only the lowest-order satellites can be observed. Satellite lines can be, due to the shake process, observed even in photon-induced x-ray spectra.

The satellites induced in collisions with protons and heavier ions have been extensively studied in the past [1–13]. In these works, the satellites were mainly used to study the ionization induced in collisions by measuring the intensity distribution of the $K\alpha L^N$ satellite lines. The $K\alpha L^N$ satellite lines of the ion-induced x-ray spectra are affected by the additional ionization of the outer shells, especially the M shell. Since the KM satellites cannot be resolved from the parent diagram line, M-shell ionization causes energy shifts and asymmetrical shape of the spectral lines. On the other hand, the photon-induced satellites, which are almost exclusively the result of the shake process, are practically free from M-shell contributions.

The measured fine structure of the $K\alpha L$ satellite lines can be used to test the theoretical predictions of the atomic structure. Extensive multiconfiguration calculations yielding energies and intensities of the transitions incorporated in the satellite lines can be used to learn more about the actual mixing of different configurations and therefore help us to better understand electron correlations in atoms. Usually photon-induced spectra are most suitable for these purposes since the measured satellite lines are not contaminated by the contribution of the KM satellites. In this work, we will show that also the proton-induced $K\alpha L$ satellite spectra are practically equivalent with the photon-induced one regarding the structure of the satellite lines when proton velocity is much higher than the velocity of the electrons within the L shell of the atom. Therefore, also proton-induced $K\alpha L$ satellite spectra yield the opportunity to study fundamental atomic properties. It even has some advantages compared to the photon-induced one since the overall intensity is higher.

In this work, we have used excellent energy resolution of our spectrometer to measure the $K\alpha L^{1,2}$ satellites of Si induced in collisions with 1–3-MeV protons. At such proton energies, the M-shell ionization causing the distortion of the satellite lines from the clean line shape observed in photoinduced spectra is almost negligible. Therefore, the structure of the $K\alpha L^{1,2}$ satellites is practically the same as in photoinduced spectra whereas the overall intensity is much higher and therefore also a second-order satellite can be clearly observed. Since no dependence of the satellite structure on the excitation energy has been observed, we have extracted the average energies and relative intensities of the main components that could be resolved within the $K\alpha L^{1,2}$ satellite lines. Besides that, the total intensities of the satellite lines relative to the diagram $K\alpha$ line have been used to obtain single L-shell electron direct ionization probabilities induced in collisions with 1–3-MeV protons. Obtained values have been

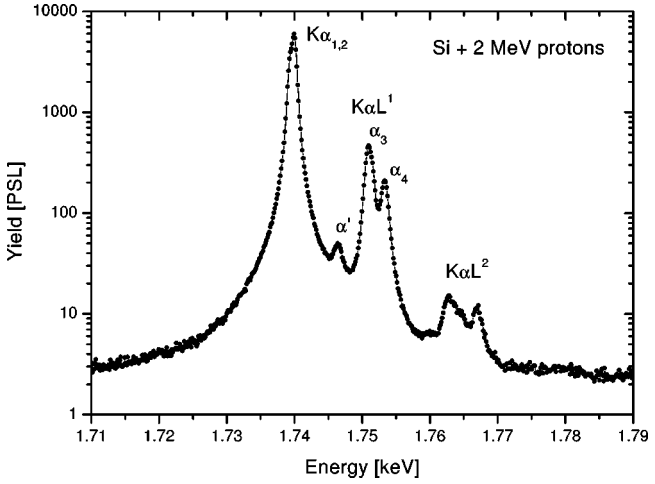

FIG. 1. High-resolution Si $K\alpha$ x-ray spectrum induced in collisions with 2-MeV protons. PSL (photostimulated luminescence) is the intensity unit used with the IP reading device and it is proportional to the number of detected photons.

compared with the theoretical values calculated within the semiclassical approximation (SCA), with the three-body classical trajectory Monte Carlo simulation (CTMC), and with the geometrical model (GM).

II. EXPERIMENT

The experiment was performed at the Microanalitical Center (MIC) of the J. Stefan Institute, Ljubljana. Protons were accelerated by a 2-MV tandem accelerator. A thick Si target was bombarded with 1-, 2-, and 3-MeV protons; beam currents of 1–2 μA were used.

The x rays emitted from the target after bombardment with protons were measured with a high-resolution crystal spectrometer. The spectrometer consists of a target holder, the target shielding which prevents the emitted x rays from reaching the detector directly, a diffraction crystal bent in Johansson geometry, and a position-sensitive detector for detection of the diffracted x rays. The whole spectrometer is closed in a $1.6\times1.3\times0.4\ \mathrm{m}^3$ stainless-steel chamber evacuated by the turbomolecular pump down to 10^{-6} mbar.

The proton incidence and x-ray emission angle relative to the target surface was 45°. Emitted photons were reflected in the first order of reflection by the ⟨100⟩ reflecting planes of the SiO_2 crystal. The crystal was bent in Johansson geometry, the radius of the Rowland circle was 100 cm, and the reflecting area was $7.5\times3\ \mathrm{cm}^2$. Reflected photons were detected by a 12.5×12.5-cm^2 Fuji imaging plate (IP) [14] with spatial resolution $100\times100\ \mu\mathrm{m}^2$. In order to reduce the background, a 6-μm mylar foil was inserted in front of the IP detector. The diffracted x rays contributed to a two-dimensional intensity pattern on the IP detector. The horizontal axis corresponds to the energy axis of the spectrum, while the vertical dimension increases the collection area. The measured two-dimensional image was projected on the horizontal axis to get the final spectrum.

The Si target was positioned well inside the Rowland circle at a distance of 37 cm in front of the diffraction crystal. In order to get the optimal energy resolution, the detector was placed on the Rowland circle where the focusing condition is fulfilled. For the Si $K\alpha$ line, the corresponding Bragg angle was 56.9° and according to that the distance of the

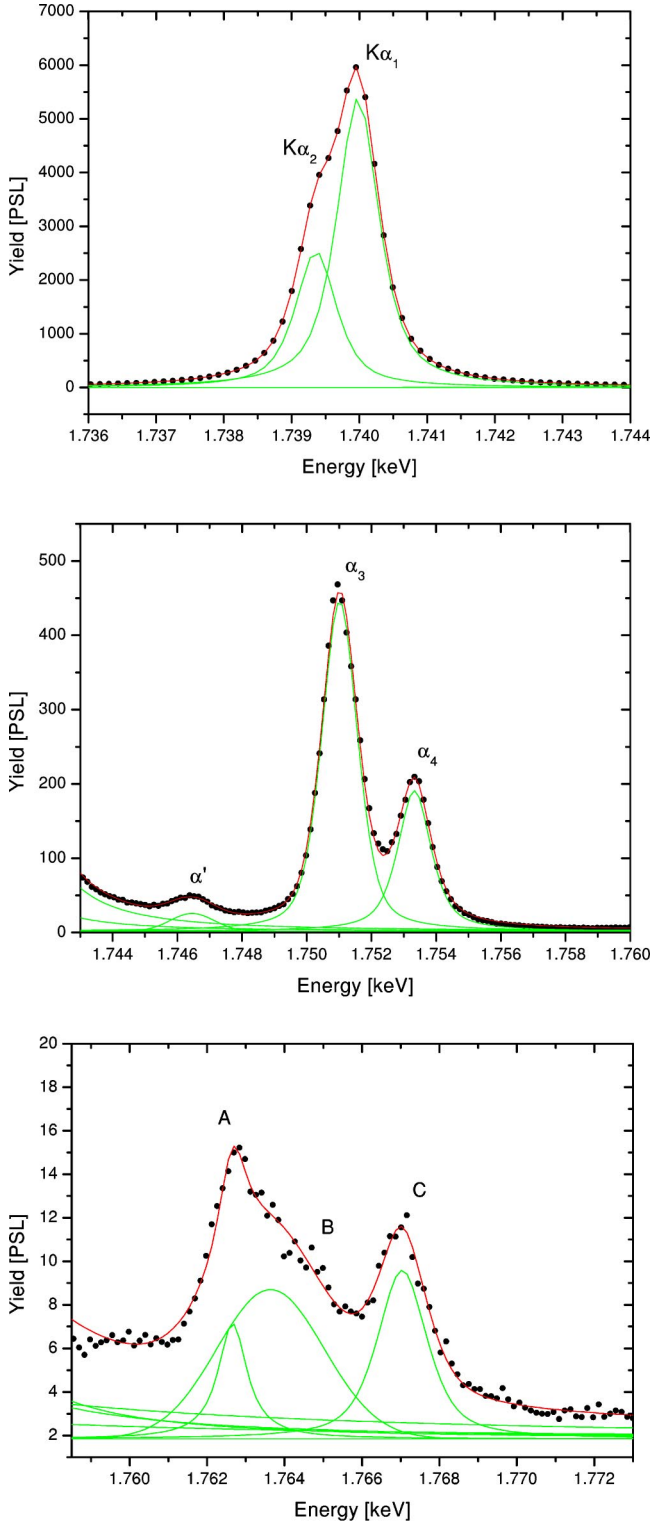

FIG. 2. High-resolution Si $K\alpha$ diagram line (top), $K\alpha L^1$ satellite line (middle), and $K\alpha L^2$ satellite line (bottom) decomposed by the fitting model explained in the text.

detector from the crystal was set to 83.7 cm. The final experimental resolution was 0.25 eV, limited mainly by the spatial resolution of the detector and the projection of the slightly curved vertical profile of the intensity pattern on the detector. This energy resolution was sufficient for clearly resolving the fine structure within the $K\alpha L^{1,2}$ satellite lines. The relatively large lateral dimensions of the detector allowed a 80-eV-wide interval to be measured at a fixed crystal-detector position set for the Si $K\alpha$ line. The position spectra were converted to the energy according to the position of the $K\alpha$ diagram line, which served as a reference line. The energy of the reference line was set to 1740.0 eV [15].

III. DATA ANALYSIS

The measured $K\alpha$ spectra exhibit two additional lines on the high-energy tail of the parent diagram line corresponding to the $K\alpha$ $(1s \rightarrow 2p)$ transitions in an atom with one and with two additional spectator vacancies in the L shell. In the case of MeV proton excitation, the single-electron L-shell ionization probability is approximately 1–2%, therefore besides the $K\alpha L^1$ satellite also the $K\alpha L^2$ can be clearly observed, whereas excitation of the higher-order satellite is almost negligible. The measured $K\alpha L^{1,2}$ satellite spectra of Si bombarded with 2-MeV protons are presented in Fig. 1.

The $K\alpha L^{1,2}$ satellite lines generally consist of many components since the different configurations of the spectator vacancies among $2s$ and $2p$ subshells and different coupling possibilities of the total angular momentum of the open subshells result in an energy splitting of both initial and final states. Since the energy shifts between the components are usually smaller then their natural linewidths, this fine structure is almost completely smeared out. The measured spectrum is always convoluted with the spectrometer response function, therefore in most of the experiments $K\alpha L$ satellite lines can only be observed as single almost symmetric lines. In our case, the contribution of the spectrometer response function was, due to excellent energy resolution, reduced as much as possible giving us the opportunity to clearly resolve three main components within the $K\alpha L^1$ and $K\alpha L^2$ satellite lines of Si induced with MeV protons. Generally, in ion-induced excitation the shape of the $K\alpha L$ satellite lines can be slightly affected by additional M-shell ionization, which may accompany ionization of the $KL^{1,2}$ states. By comparing the measured spectra excited with 1-, 2-, and 3-MeV protons, we have found this contribution to be negligible since the shape of the $K\alpha L^{1,2}$ satellite lines was independent of the proton energy.

In order to determine the parameters of the three main components within the $K\alpha L^1$ and $K\alpha L^2$ satellite lines, we have fitted them with three pseudo-Voigt lines which are linear combinations of Lorentzian and Gaussian functions, representing the natural line shape and the instrumental response, respectively. All parameters of the three lines were not constrained in the fitting procedure. The diagram $K\alpha$ line was fitted with two pseudo-Voigt lines with equal widths. An example of such a fit is presented in Fig. 2.

Besides the energies and intensities of the components within the $K\alpha L^{1,2}$ satellite lines, we were also interested in the total intensity of the satellite lines relative to the diagram $K\alpha$ line. Therefore, we needed to apply several experimental corrections of the intensity ratio after the fitting procedure. First the relative satellite yields were corrected for the x-ray absorption in the mylar foil and for the crystal reflectivity. For the calculation of the absorption correction, the x-ray attenuation coefficients of Thinh and Leroux [16] were used. For the crystal reflectivity correction we have taken the reflectivity of the ideal mosaic crystal with absorption in the crystal [17]. Since both these corrections generally depend on the energy difference between the satellite and the diagram line, which was very small ($\Delta E = 11.6$ eV for the $K\alpha L^1$ line and 22.7 eV for the $K\alpha L^2$ line), these effects gave a total correction of 3.1% for the total intensity of the $K\alpha L^1$ line relative to the $K\alpha$ diagram line. The effects of x-ray absorption and the crystal reflectivity on the relative intensities of the components within each satellite line were negligible.

Because of the thick targets used, we had to account for the proton stopping and x-ray absorption in the target. The measured thick target satellite yields were converted into their respective thin target values by the use of correction factor, which can be written as

$$F_{\mathrm{corr}} = \frac{\sigma^{\mathrm{SCA}}_{KL^1}(E_0)/\sigma^{\mathrm{SCA}}_{KL^0}(E_0)}{\int_0^R \sigma^{\mathrm{SCA}}_{KL^1}(E(x))\exp(-\mu^{KL^1}x)dx / \int_0^R \sigma^{\mathrm{SCA}}_{KL^0}(E(x))\exp(-\mu^{KL^0}x)dx}, \tag{1}$$

where σ_{KL^0} and σ_{KL^1} are the ionization cross sections for the KL^0 and KL^1 state, respectively, $E(x)$ is the proton energy as a function of penetration depth, E_0 is the proton impact energy, R is the range of protons, and μ is the x-ray-absorption coefficient in the Si target. We have used cross sections calculated within the independent electron model incorporating single K- and L-shell ionization probabilities calculated with the semiclassical approximation (SCA). The $E(x)$ function was calculated using the stopping powers of Ziegler and Manoyan [18] and the x-ray attenuation coefficients for Si were obtained from the tables of Thinh and Leroux [16]. The final thick target correction factors for the KL^1 satellite yield relative to the $K\alpha$ diagram line are tabulated together with the final KL^1 vacancy yield in Table III (a

TABLE I. Energies and relative intensities of the three main components (α', α_3, and α_4) within the $K\alpha L^1$ satellite and the total overall intensity of the $K\alpha L^1$ line relative to the $K\alpha$ diagram one.

	$E_p=1$ MeV	$E_p=2$ MeV	$E_p=3$ MeV	Average
$E(\alpha')$ (eV)	1746.6±0.1	1746.5±0.1	1746.6±0.1	1746.57±0.03
$E(\alpha_3)$ (eV)	1751.2±0.1	1751.0±0.1	1751.1±0.1	1751.10±0.06
$E(\alpha_4)$ (eV)	1753.5±0.1	1753.3±0.1	1753.5±0.1	1753.43±0.07
$Y_r(\alpha')$ (%)	2.7±0.3	3.6±0.3	2.8±0.3	3.0±0.3
$Y_r(\alpha_3)$ (%)	68.3±0.9	67.1±0.9	66.4±0.9	67.3±0.6
$Y_r(\alpha_4)$ (%)	29.0±0.8	29.3±0.8	30.8±0.8	29.7±0.6
Y (KL^1/KL^0) (%)	18.6±1.0	13.2±0.7	8.5±0.8	

3.1% correction due to absorption in mylar and crystal reflectivity is already incorporated in the tabulated values).

IV. RESULTS AND DISCUSSION

The energies and relative intensities of the three main components within the $K\alpha L^1$ and $K\alpha L^2$ satellite lines and the overall intensities of both satellites relative to the $K\alpha$ diagram line determined from the fitting procedure are given in Tables I and II. Tabulated are the values for each of the three proton energies used for target excitation. From the tabulated values we can see that the energies and relative intensities of the fine-structure components within each satellite line do not depend on the energy of proton excitation.

A. Energies

Our measured $K\alpha L^1$ satellite energies can be compared to the theoretical values presented in the paper of Deutsch [19]. Deutsch has calculated the average $K\alpha L^1$ satellite energy shift from the center of the $K\alpha$ diagram line for atoms having $10 \leqslant Z \leqslant 32$. His calculations employing nonrelativistic Hartree-Fock energies yielding 10.8 eV for the Si $K\alpha L^1$ line. In his work, he has also presented values calculated with the hydrogenic analytical model of Burch *et al.* [20] using both Hartree-Fock derived and Slater-rule screening constants. These two types of screening yield values of 15.5 and 16.4 eV, respectively. The Burch analytical model has been extended by Bhattacharya *et al.* [21] using the self-consistent-field functions. Bhattacharya is giving 12.5 eV for Si, which is closest to our experimental value 11.9 eV. Therefore, good agreement between the Bhattacharya theoretical values and experimental values measured by photons, electrons, and ions [19] has been confirmed also by our measurements. Deutsch is claiming that the Hartree-Fock (HF) calculations agree with experiments up to $Z=16$. Our measured value shows that already by $Z=14$ the HF value underestimates the experimental one.

B. Intensities

Relative intensities of the components within the $K\alpha L^1$ and $K\alpha L^2$ satellites are given in Tables I and II. Our measured value of $Y_r(\alpha_4)/Y_r(\alpha_3)$, which is 0.44 ± 0.01, is in agreement with the value obtained by Mauron *et al.* [22]. They have measured the photo induced $K\alpha L^1$ satellite line and obtained 0.452 ± 0.006. For the $K\alpha L^2$ satellite line, no values for the relative intensities were found in the literature.

Besides relative intensities of the main components within each satellite line, also overall intensities of the satellite lines relative to the parent $K\alpha$ diagram line are given in Tables I and II. Since these values directly reflect the L-shell ionization probability in near-central collisions of protons with target atoms, they depend on the energy of the protons used for excitation. In this work, we have used the total $K\alpha L^1$ satellite intensities to extract direct L-shell ionization probabilities for the measured collisions. Since the satellite lines can be produced either by direct ionization due to Coulomb interaction of electrons with protons or by the shake process, our measured satellite lines incorporate both contributions. In order to obtain direct L-shell ionization probabilities, the measured intensity needs to be corrected for the shake contribution. In the recent work of Mauron *et al.* [22], they have

TABLE II. Energies and relative intensities of the three main components (denoted simply as A, B, and C) within the $K\alpha L^2$ satellite and the total overall intensity of the $K\alpha L^2$ line relative to the $K\alpha L^1$ satellite one.

	$E_p=1$ MeV	$E_p=2$ MeV	$E_p=3$ MeV	Average
$E(K\alpha L^2_A)$ (eV)	1762.8±0.3	1762.7±0.3	1762.8±2.4	1762.75±0.04
$E(K\alpha L^2_B)$ (eV)	1763.8±1.0	1763.6±0.6	1763.7±0.7	1763.67±0.05
$E(K\alpha L^2_C)$ (eV)	1767.2±0.3	1767.0±0.3	1767.2±0.6	1767.11±0.07
$Y_r(K\alpha L^2_A)$ (%)	18.3±2.7	15.8±2.4	18.1±2.7	17.3±0.8
$Y_r(K\alpha L^2_B)$ (%)	50.2±7.5	49.8±7.5	49.6±7.5	49.9±0.2
$Y_r(K\alpha L^2_C)$ (%)	31.5±3.2	34.4±3.1	32.3±3.3	32.8±0.9
Y (KL^2/KL^1) (%)	5.3±0.8	4.3±0.6	3.9±0.6	

TABLE III. Thick target correction factor, x-ray yield ratios, initial vacancy yield ratios, and single L-shell electron direct ionization probabilities for the measured near-central collisions.

	F_{corr}	$X(K\alpha L^1)/X(K\alpha L^0)$	$I(KL^1)/I(KL^0)$	p_L (units of 10^{-2})
$E_p=1$ MeV	0.791	$10.2\%\pm0.6\%$	$10.6\%\pm1.7\%$	1.31 ± 0.21
$E_p=2$ MeV	0.834	$6.2\%\pm0.3\%$	$6.4\%\pm1.0\%$	0.79 ± 0.13
$E_p=3$ MeV	0.907	$2.5\%\pm0.2\%$	$2.6\%\pm0.5\%$	0.32 ± 0.06

measured the intensity of the Si $K\alpha L^1$ shake satellite to be 5.72% relative to the $K\alpha$ diagram line. This value has been subtracted from our $K\alpha L^1$ satellite intensity in order to obtain direct ionization contribution solely. Since no data about the $K\alpha L^2$ shake satellite were found, we have omitted the $K\alpha L^2$ satellite in the extraction of the direct L-shell ionization probabilities induced in measured collisions.

First of all we needed to deduce the primary vacancy yield from the measured x-ray yields. The satellite line intensities are related to the primary vacancy yields by the following equations:

$$X(K\alpha L^0)=[I(K\alpha L^0)+RI(K\alpha L^1)]\omega^0_{K\alpha}, \tag{2}$$

$$X(K\alpha L^1)=[I(K\alpha L^1)(1-R)]\omega^1_{K\alpha}, \tag{3}$$

where X denotes the x-ray satellite line intensity, I is the initial vacancy yield, and $\omega_{K\alpha}$ is the partial fluorescence yield for the $K\alpha$ transition. The factor R is the rearrangement factor which gives the probability that the L-shell vacancy in the atom has been promoted to a higher shell within the lifetime of the KL ionized state. The rearrangement factor for the L shell can be written as

$$R=\sum_{2s,2p} w_{2s,2p}\frac{\Gamma^{\text{Aug}}_{2s,2p}+\Gamma^{\text{rad}}_{2s,2p}}{\Gamma_{2s,2p}+\Gamma_K}, \tag{4}$$

where Γ_K and $\Gamma_{2s,2p}$ represent the total widths for the K shell and $2s,2p$ subshells, respectively. $\Gamma^{\text{Aug,rad}}$ represent the Auger and radiative widths and the $w_{2s,2p}$ weighting factors reflecting the probability that the L-shell vacancy has been created either in a $2s$ or $2p$ subshell. According to the SCA calculated $2s$ and $2p$ single-electron ionization probabilities, we can set w_{2s} and w_{2p} to 0.256 and 0.744, respectively. The $\Gamma_{2s,2p}$ level widths were taken to 0.9 and 0.05 according to Campbell and Papp [23]. The Auger widths for the $2s$ and $2p$ subshells were taken to 0.04 and 0.05 [24], whereas the radiative widths for the $2s,2p$ subshells can be neglected. The Γ_K value in Eq. (3) needs to be corrected due to an additional L-shell vacancy present in the atom during the deexcitation process. The Γ_K level width from Campbell and Papp (0.425 eV) has been corrected according to the procedure explained in [25], yielding the value 0.320 eV. Using these values, Eq. (4) yields 0.109 ± 0.033 for the rearrangement factor. The error of the rearrangement factor has been calculated taking into account 15%, 10%, and 30% uncertainties for the Γ_K, Γ_{2s}, and Γ_{2p} level widths according to Campbell and Papp [23]. The uncertainties for the Γ^{Aug}_{2s} and Γ^{Aug}_{2p} have been estimated to 30%.

In order to finally obtain the primary vacancy yield according to Eqs. (2) and (3), we need also the partial fluorescence yield for the $K\alpha$ transition in doubly ionized atoms. We have used values calculated by Tunnel and Bhalla [26]. They are giving 0.053 for the singly $1s$ ionized Si atom and 0.065 and 0.057 for the $1s2s$ and $1s2p$ ionized Si atom. It is important to notice that Tunnel and Bhalla are giving total K-shell fluorescence yields whereas we are dealing with partial yield for the $K\alpha$ transition only. Since the $K\alpha$ radiative transition represents 98.3% of the total Γ^{rad}_K [27], we can simply equal the partial $K\alpha$ and total K fluorescence yields using the original values from Tunnel and Bhalla. In order to obtain $\omega^1_{K\alpha}$ fluorescence yield for the KL^1 ionized state used in Eq. (3), we need to know the relative L-shell vacancy population among the $2s$ and $2p$ subshells at the moment of $K\alpha$ x-ray emission. According to the procedure presented in [25], we have obtained 0.07 and 0.93 for the relative vacancy population of the $2s$ and $2p$ subshell yielding the final $\omega^1_{K\alpha}$ value of 0.058. Using the calculated R, $\omega^0_{K\alpha}$, and $\omega^1_{K\alpha}$ values we have extracted the primary KL^1 vacancy yields from the measured $K\alpha L^1$ x-ray yields according to Eqs. (2) and (3).

Within the independent electron approximation, the KL^N primary vacancy yield can be written as

$$I(KL^N)\propto\binom{8}{N}p_L^N(1-p_L^N)^{8-N}, \tag{5}$$

where p_L is the single-electron ionization probability for the near-zero impact parameter averaged over the L subshells. Using Eq. (5), one can express p_L as a function of the initial yield ratio

$$\frac{I(KL^1)}{I(KL^0)}=\frac{8p_L}{(1-p_L)}\Rightarrow p_L=\frac{I(KL^1)/I(KL^0)}{8+[I(KL^1)/I(KL^0)]}. \tag{6}$$

The final KL^1 vacancy yields extracted from the measured $K\alpha L^1$ x-ray yields and the average single L-shell electron ionization probabilities calculated according to Eq. (6) are tabulated in Table III.

Among the theories that describe ionization by charged projectiles and employ a quantum description of the atom, only the SCA allows calculation of the ionization probabilities as a function of impact parameter. In the present study, we calculated the direct ionization probabilities according to the first-order SCA model of Trautmann and Rösel (IONHYD code) [28,29]. The latter employs classical hyperbolic trajectories and uses hydrogenlike Dirac electron wave functions. The effective charge of the target atom was calculated according to the method of Slater to account for screening ef-

fects. Binding energies of the separated atom model were employed. Multipoles up to the order $l=5$ were considered in the calculations. Usually the ionization probabilities for near-central collisions obtained from satellite measurements are compared to the theoretical values calculated at some effective impact parameter (b_{eff}), which in the case of KL ionization is chosen so that the $p_K(b)b_{\mathrm{eff}}$ is maximized. In our calculations, b_{eff} was set to 4000 fm.

Besides the SCA calculations, the direct ionization probabilities for the measured collisions have been calculated also with the three-body classical trajectory Monte Carlo model (CTMC). The three-body, three-dimensional CTMC calculations were performed as described in [30] and [31]. The calculations incorporated the bare projectile, an active atomic electron, and the remaining ion. For the description of the interaction between them, a potential model based on Hartree-Fock calculations as developed by Green [32] was used. The initial parameters were the same as those developed by Reinhold and Falcon [33]. They were chosen randomly at relatively large internuclear separations, where the interaction between the projectile and the target atom is negligible. The initial conditions were set from the ensemble, which is constrained to an initial binding energy of the L-shell target electron. For the given initial parameters, Newton's equations of motion were integrated with respect to time as an independent variable by the standard Runge-Kutta method until large separations of the colliding particles were attained. For each investigated collision, 20 000 individual trajectories were calculated.

Another possibility to calculate direct ionization probabilities at near-zero impact parameter is the geometrical model (GM) of Sulik *et al.* [34], which is based on the binary encounter approximation. In the GM approach, we consider a projectile at a velocity higher than the orbital electron velocity passing through the target atom along a straight line at zero impact parameter. The energy transferred to the target electron is a unique function of the projectile-electron impact parameter defining a cylinder around the projectile trajectory in which the target electron acquires the amount of energy needed for ionization. The probability of ionization is simply given as the charge-density fraction of one electron cut out by the cylinder. The L-shell direct ionization probabilites of interest were also computed with the geometrical model incorporating the hydrogenic single-electron density distributions.

A comparison of experimental values with the theoretical curves is presented in Fig. 3. As expected, the SCA model employing a quantum description of the L-shell electrons yields values closest to the experimental ones but still underestimates them, which is probably a consequence of using the hydrogenic wave functions for the $2s,2p$ electrons as pointed out in [12]. The CTMC values as well as the GM ones reproduce the energy dependence but overestimate the experimental results quite a bit.

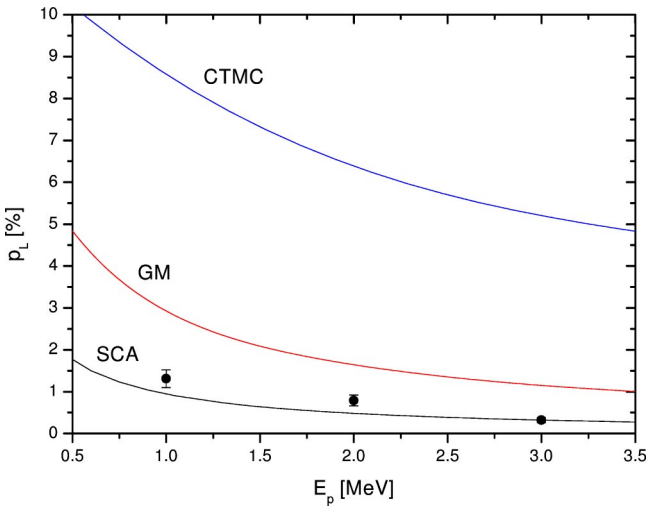

FIG. 3. Single L-shell electron direct ionization probabilities for the near-zero impact parameter as a function of the proton energy. The experimental data are compared with the calculations within the SCA model [28,29], the CTMC model [30,31], and the GM model [34].

V. SUMMARY AND CONCLUSION

The Si $K\alpha L^{1,2}$ satellites induced in collisions with 1-, 2-, and 3-MeV protons have been measured with the high-resolution crystal spectrometer in Johannsson geometry. Experimental energy resolution below the natural linewidth of the Si $K\alpha$ line enabled us precisely to determine the energies and relative intensities of the three main components that could be resolved within each satellite line. It has been demonstrated that the latter do not depend on the proton energy; furthermore, the equivalence with the photon-induced spectra has been suggested. The total overall intensities of the $K\alpha L^1$ satellite line have been used to extract the single-electron direct ionization probabilities averaged over the three L subshells induced in near-central collisions with protons. The experimental values have been compared to the theoretical values calculated within the semiclassical (SCA) model, the three-body classical trajectory Monte Carlo calculation (CTMC), and the geometrical model incorporating the classical binary encounter collision model.

The measured energies of the α', α_3, and α_4 lines within the $K\alpha L^1$ satellite support the calculation of Bhattacharya *et al.* [21], whereas our values show that already for $Z=14$ the HF calculation of the satellite energy underestimates the experimental one. Comparison of the ionization probabilities with the theoretical values favors the SCA calculation over the CTMC and GM model, even though the SCA also underestimates the measured values.

ACKNOWLEDGMENTS

The author thanks K. Tökési for providing the CTMC calculated values. He also wishes to thank P. Pelicon and K. Ravnikar for providing very good beam conditions and M. Kobal for fruitful discussions. This work was supported by the Slovenian Ministry of Education, Science and Sport through the research program ''Low Energy Physics'' (PO-0521-0106-02).

[1] R. L. Kauffman, J. H. McGuire, and P. Richard, Phys. Rev. A **8**, 1233 (1973).
[2] T. K. Li, R. L. Watson, and J. S. Hansen, Phys. Rev. A **8**, 1258 (1973).
[3] R. L. Watson, F. E. Jenson, and T. Chiao, Phys. Rev. A **10**, 1230 (1974).
[4] V. Dutkiewitcz, H. Bakhru, and N. Cue, Phys. Rev. A **13**, 306 (1976).
[5] K. W. Hill, B. L. Doyle, S. M. Shafroth, D. H. Madison, and R. D. Deslattes, Phys. Rev. A **13**, 1334 (1976).
[6] R. L. Watson, B. I. Sonobe, J. A. Demarest, and A. Langenberg, Phys. Rev. A **19**, 1529 (1979).
[7] B. Perny, J.-Cl. Dousse, M. Gasser, J. Kern, Ch. Rhême, P. Rymuza, and Z. Sujkowski, Phys. Rev. A **36**, 2120 (1987).
[8] P. Rymuza, Z. Sujkowski, M. Carlen, J.-Cl. Dousse, M. Gasser, J. Kern, B. Perny, and Ch. Rhême, Z. Phys. D: At., Mol. Clusters **14**, 37 (1989).
[9] P. Rymuza, T. Ludziejewski, Z. Sujkowski, M. Carlen, J.-Cl. Dousse, M. Gasser, J. Kern, and Ch. Rhême, Z. Phys. D: At., Mol. Clusters **23**, 71 (1992).
[10] B. Boschung, M. W. Carlen, J.-Cl. Dousse, B. Galley, Ch. Herren, J. Hoszowska, J. Kern, Ch. Rhême, T. Ludziejewski, P. Rymuza, Z. Sujkowski, and Z. Halabuka, Phys. Rev. A **52**, 3889 (1995).
[11] D. F. Anagnostopoulos, G. L. Borchert, and D. Gotta, J. Phys. B **25**, 2771 (1992).
[12] M. Kavčič, Ž. Šmit, M. Budnar, and Z. Halabuka, Phys. Rev. A **56**, 4675 (1997).
[13] M. Kavčič, M. Budnar, A. Mühleisen, P. Pelicon, Ž. Šmit, M. Žitnik, D. Castella, D. Corminboeuf, J.-Cl. Dousse, J. Hoszowska, P. A. Raboud, and K. Tökési, Phys. Rev. A **61**, 052711 (2000).
[14] J. Miyahira, K. Takahashi, Y. Amemiya, N. Kamiya, and Y. Satow, Nucl. Instrum. Methods Phys. Res. A **246**, 572 (1986).
[15] J. A. Bearden, Rev. Mod. Phys. **39**, 78 (1967).
[16] T. P. Thinh and J. Leroux, X-Ray Spectrom. **8**, 85 (1979).
[17] R. W. James, *The Optical Principles of Diffraction of X-rays* (Bell, London, 1950).
[18] J. F. Ziegler and J. Manoyan, Nucl. Instrum. Methods Phys. Res. B **35**, 215 (1988).
[19] M. Deutsch, Phys. Rev. A **39**, 1077 (1989).
[20] D. Burch, L. Wilets, and W. E. Meyerhof, Phys. Rev. A **9**, 1007 (1974).
[21] J. Bhattacharya, U. Laha, and B. Talukdar, Phys. Rev. A **37**, 3162 (1988).
[22] O. Mauron, J.-Cl. Dousse, J. Hoszowska, J. P. Marques, F. Parente, and M. Polasik, Phys. Rev. A **62**, 062508 (1988).
[23] J. L. Campbell and T. Papp, At. Data Nucl. Data Tables **77**, 1 (2001).
[24] J. L. Campbell (private communication).
[25] M. Kavčič, M. Budnar, and J. L. Campbell, Nucl. Instrum. Methods Phys. Res. B **196**, 16 (2002).
[26] T. W. Tunnel and C. P. Bhalla, Phys. Lett. **86A**, 13 (1981).
[27] J. H. Scofield, At. Data Nucl. Data Tables **14**, 121 (1974).
[28] D. Trautmann and F. Rösel, Nucl. Instrum. Methods **169**, 259 (1980).
[29] D. Trautmann and F. Rösel, Nucl. Instrum. Methods Phys. Res. **214**, 21 (1983).
[30] K. Tokesi and G. Hock, J. Phys. B **29**, L119 (1996).
[31] B. Sulik, K. Tokesi, Y. Awaya, T. Kambara, and Y. Kanai, Nucl. Instrum. Methods Phys. Res. B **154**, 286 (1999).
[32] A. E. S. Green, Adv. Quantum Chem. **7**, 221 (1973).
[33] C. O. Reinhold and C. A. Falcon, Phys. Rev. A **33**, 3859 (1986).
[34] B. Sulik, I. Kádár, S. Ricz, D. Varga, J. Végh, G. Hock, and D. Berényi, Nucl. Instrum. Methods Phys. Res. B **28**, 509 (1983).